Structural insights into charge pair interactions in triple helical collagen-like proteins *

Jorge A. Fallas[1], Jinhui Dong[2], Yizhi J. Tao[2] and Jeffrey D. Hartgerink[1,3]

Departments of [1]Chemistry, [2]Biochemistry and Cell biology and [3]Bioengineering
Rice University, Houston, Texas 77005

To whom correspondence may be addressed: Jeffrey D. Hartgerink, Ph.D., 6100 Main Street, MS-602, Houston, TX 77005. Fax: 713-348-4201; E-mail: jdh@rice.edu

Supporting Information

Peptide Synthesis and Purification- The peptides were synthesized in house with an Advanced Chemtech Apex 396 solid phase peptide synthesizer using standard Fmoc chemistry and a Rink MBH amide resin. During the automated procedure a manual addition of 2 equivalents ^{15}N-labelled glycine, purchased form Cambridge Isotope Laboratories, was carried out in position 12. The final products are N-terminally acetylated and C-terminally amidated to provide increased thermal stability. Purification was performed on a Varian PrepStar220 HPLC using a preparative reverse phase C-18 column with a linear gradient of water and acetonitrile each containing 0.5 % TFA and analyzed by ESI-TOF mass spectrometry on a Bruker microTOF instrument (Fig. S1).

*Crystallization and Data Collection-*The pure and lyophilized **KGE** peptide powder was dissolved at concentrations of 8, 10, 12, 15 mg/ml in water and pH adjusted to a value of 7.0 using 0.1 M sodium hydroxide. The peptide was crystallized using the hanging drop vapor diffusion method by mixing 1 μl of the peptide solution with 1 μl of 50% tacsimate solution, purchased from Hampton Research. Crystals grew as thin plates at pH values ranging from 5.9 – 7.1 in approximately 3 days. Crystals at pH 6.4 and peptide concentration of 12 mg/ml were chosen for data acquisition. The sample was flash-cooled in a N_2 cryostream at 100K using 7.5 % glycerol in the mother liquor as cryoprotectant. Data was collected at 1.54 Å using a Rigaku RUH3R rotating anode X-ray generator with a Rigaku R-axis IV++ detector in 0.5° wedges. The crystals diffracted to 1.68 Å and were indexed to a triclinic unit cell, space group P1, with dimensions: a = 14.03 Å, b = 23.82 Å, c = 67.66 Å, α = 95.0° , β = 94.7° and γ = 94.9° using the hkl2000 software(5).

Circular Dichroism- All CD experiments were performed with a Jasco J-810 spectropolarimeter equipped with a Peltier temperature control system. 300 μM samples were prepared in 10 mM phosphate buffer at pH 7 and incubated overnight at room temperature. Spectra were acquired between 215-250 nm and the maximum around 222 nm, was monitored during unfolding curves. Melting experiments were performed from 5 to 85 °C with a heating rate of 10 °C/hr. The first derivative of the melting curve was taken in order to determine the melting temperature (T_m) of the sample, which we define as the minimum in the derivative graph. The molar residual ellipticity (MRE) is calculated from the measured ellipticity using the equation:

$$[\theta] = \frac{\theta \times m}{c \times l \times n_r}$$

where θ is the ellipticity in mdeg, m is the molecular weight in g/mol, c is the concentration in mg/mL, l is the pathlength of the cuvette in cm, and n_r is the number of amino acids in the peptide.

Structure Determination and Refinement- The structures were solved by molecular replacement using the epmr software(6). Several search models were tried for the **KGE** crystal but a modified version of the structure 1QSU(7) containing alanine mutations at positions 13, 14 and 16 and reduced from ten to eight triplets in length yielded the highest correlation coefficient (CC = 0.722, R-factor=0.45) for the with two anti-parallel triple helices in the asymmetric unit. THE **KGD** structure was solved using a modified version of the **KGE** structure containing alanine mutations at position 13 of each chain and was also found to contain two anti-parallel triple helices in the asymmetric unit (CC = 0.75, R-factor=0.42).   The initial phases were improved by rigid body refinement followed by rounds of simulated annealing and anisotropic B-factor refinement starting at 3.0 Å resolution and gradually increasing using the CNS suite(8). The models were rebuilt in coot(9) when the composite omit map showed clear density for the missing side chains. After further rounds of refinement with increasing resolution water addition was begun in CNS since it is known that triple helical peptides are often associated with an extensive water network that contributes significantly to the total scattering of the asymmetric unit(7)(10). After each round of automated water picking further rounds of atomic position, temperature factor refinement and model rebulding were carried out with increasing resolution until the limiting value of 1.68 Å was reached for the **KGE** structure and 2.01 Å for the **KGD** structure. The final **KGE** model contains 935 peptide atoms and 219 water molecules. The C-terminal glycine of the B chain was not modeled due to poor density in that region. The final **KGD** model contains 915 peptide atoms and 180 water molecules. The N-terminal proline and hydroxyproline of the D chain were not modeled due to poor density in that region. The final CNS models were subjected to TLS refinement in refmac(11), where each of the six peptide chains in the asymmetric unit was treated as a rigid body in the procedure. The final **KGE** structure has an R_{work} / R_{free} value of 18.9 / 20.7 % and the final **KGD** structure has an R_{work} / R_{free} value of 23.9 / 25.0 % .

NMR Spectroscopy- All NMR experiments were recorded in an 800 MHz Varian spectrometer equipped with a triple resonance probe at 5° C. The spectra were processed using NMRpipe(12) and analyzed using ccpnmr(13). Square Cosine bell window functions were used as apodization functions and the data was zero-filled to the next power of two in both dimensions.   Drift corrections were applied when necessary. Samples of each peptide were prepared with a total peptide concentration of 3 mM, determined by mass, in a 9:1 ratio of H_2O to D_2O and 10 mM phosphate buffer at neutral pH. Each sample was characterized using 2D total correlated spectroscopy (TOCSY), nuclear Overhauser effect spectroscopy (NOESY), $^1H,^{15}N$-heteronuclear single quantum coherence (HSQC) and 3D NOESY-^{15}N-HSQC experiments. The sequential assignment procedure was carried out using a combination of $^1H,^1H$-TOCSY and $^1H,^1H$-NOESY experiments. All sequential NOEs from the NH of residue *i* to the $C_\alpha H$ of residue *i-1* are observed in the guest region. The chain register assignment was determined using the resonance between $Lys^C(H_\alpha)$ and $Glu^A(NH)$ or $Asp^A(NH)$, which, due to structural constraints, only occurs between the lagging and leading strands. The side chain resonances were assigned using a combination of $^1H,^{15}N,^1H$-NOESY-HSQC experiments. TOCSY spectra with a 30 ms spinlock duration at 8 kHz were acquired with a total of 1360 complex points recorded in 8 scans for the

directly acquired dimension while 480 increments were used in the indirect dimension. NOESY spectra with a 75 ms mixing time were acquired with a total of 1360 complex points recorded in 8 scans for the directly acquired dimension while 480 increments were used in the indirect dimension. A square spectral window of 8000 Hz was used for all spectra. A total of 1192 complex points in 32 scans for the direct dimension and 50 increments in the indirect dimension were acquired for the ^{1}H,^{15}N-HSQC experiments using a spectral window of 8000 Hz in the hydrogen dimension and 1620 Hz in the nitrogen dimension. The data was processed by zero filling to the next power of two and cosine bell apodization functions were applied in both dimensions. For the 3D NOESY-^{15}N-HSQC spectra a mixing time of 100 ms was used and a total of 1360 complex points in 8 scans for the direct dimension, 120 increments for the first indirect dimension and 12 increments for the second indirect dimensions were acquired using a spectral window of 8000 Hz for direct dimension, 1376 for the hydrogen indirect dimension and 809 Hz for the nitrogen indirect dimension. The data was processed by zero filling to the next power of two and cosine bell apodization functions were applied in all dimensions. Forward backwards linear prediction was used.

Stereospecific Assigments- The stereo-specific assignment of methylene protons in the guest region was done qualitatively using the cross peak intensity of the protons in question and other anchor atoms in the peptide with unambiguous chemical shift assignments. In the following section we will describe the process for several particular cases and mention what other protons were assigned using similar distance constraints. In general, several assumptions were made: i) diasterotopic protons with unique chemical shifts for each their methylene protons adopt a rigid conformation and preferentially populate a particular side-chain rotamer ii) only rotamers that avoid steric clashes with the triple helical backbone are populated and iii) only trans and gauche conformations are allowed for each c dihedral. Most NOEs used could be resolved in the 2D ^{1}H,^{1}H-NOESY spectrum, however in some cases the 3D ^{1}H,^{15}N,^{1}H-NOESY-NHSQC spectrum was used to avoid ambiguity.

The easiest diasterotopic protons to assign are the glycine a-protons. Because of the backbone dihedrals observed in the triple helix Ha3 is closer to the glycine amide proton and thus produces a stronger NOE. This fact can be used to assign all the backbone diasterotopic atoms in the guest region.

The assignment of diasterotopic β-protons was done following the procedure described by Clore *et al.* (14) using the intra-residue NOEs between the β-protons and the backbone amide and α-proton expected for the allowed values of the χ_1 dihedral. Table S4 shows the relative intensity expected for the different cross peaks based on the distance measured in the model for E37. If the distance between the anchor atom (either Hα or NH) and each of the β-methylene protons is similar an "~" is presented in the table for both pairs, indicating that NOEs with comparable intensities are expected. On the other hand, if one of the β-protons is closer to the anchor atom then an "+" is presented, signifying that a stronger NOE is expected for that pair, and "–" in the complementary case. The qualitative assignment of the observed NOEs is presented in the last column for comparison. Using this information is possible to assign both the conformer of the χ_1 dihedral and the identity of each of the β-protons. An identical analysis is used to assign residues E13 and E61 in the **KGE** spectra as well as D13, D37 and D61 in the **KGD** spectra.

The γ-protons in for the glutamates were assigned using a similar procedure with one aditional constraint, the χ_1 dihedral was assumed fixed at the value previously determined. In this

case the anchor atoms used for the assignment are Hβ_2 and NH. The same conventions as above were utilized and the results for E37 are summarized in table S5. The same analysis for E61 leads to the same conclusions.

      The γ-protons in for the lysine residues in both peptides are more challenging to assign given the lack of unambiguous information for the χ_1 dihedral in that residue from NOE data. In order to overcome this problem we utilized geometrical constraints derived from the observed NOEs. For instance, only 4 out of the 81 rotamaters available to the lysine side-chain allow for the observed NOE Glu37(NH)-Lys11(H$_\varepsilon$) while simultaneously avoiding clashes with the peptide backbone in triple helical conformation. All of these four conformers have identical χ_1 and χ_2 dihedrals, in the trans conformation. Using this assumption and the relative intensity of the inter-residue Lys11(H$_{g2,3}$)-Gly12(NH) NOEs the stereospecific assignment is possible. A comparable analysis using the pair of inter-strand Lys11(H$_{\varepsilon1,2}$)-Glu37(NH) resonances and the intra-residue Lys11(H$_{g2}$)- Lys11(H$_{\varepsilon1,2}$) resonances can be used to assign the ε-protons.

NMR Ensemble Calculation- For the **KGE** peptide the ensemble was generated starting from its crystal structure and for the **KGD** peptide the glutamic acid residues were mutated to aspartic acid using using PyMOL(15). Beacause not enough experimental constraints are available for a traditional NMR structure determination conformational sampling was achieved by running langevin dynamic simulations in implicit solvent for 2.5 ns at 248.15, 298.15, 348.15 and 398.15 K using the AMBER99(16) force field. Weak harmonic constraints were placed at the terminal residues(17) and parameters to bias the hydroxyproline towards the observed ring pucker were used(18) to provide a more efficient sampling of relevant triple helical conformations. Snapshots were taken every 2.5 picoseconds along the trajectory and sorted according to their energy. The 125 lowest energy conformations from each temperature were then subjected to a minimization procedure including distance constraints derived from NOE data. The distance constraints were generated from the acquired NOESY spectra, assuming a r^{-6} proportionality between intensity and distance and using the intensity of the resonance between the acidic amide proton and the glycine HB2 proton in the middle chain together with its distance from the crystal structure as a reference. Only constraints involving the charged residues were used during the minimization procedure. The 100 lowest energy structures after the minimization step were selected for the final ensemble.
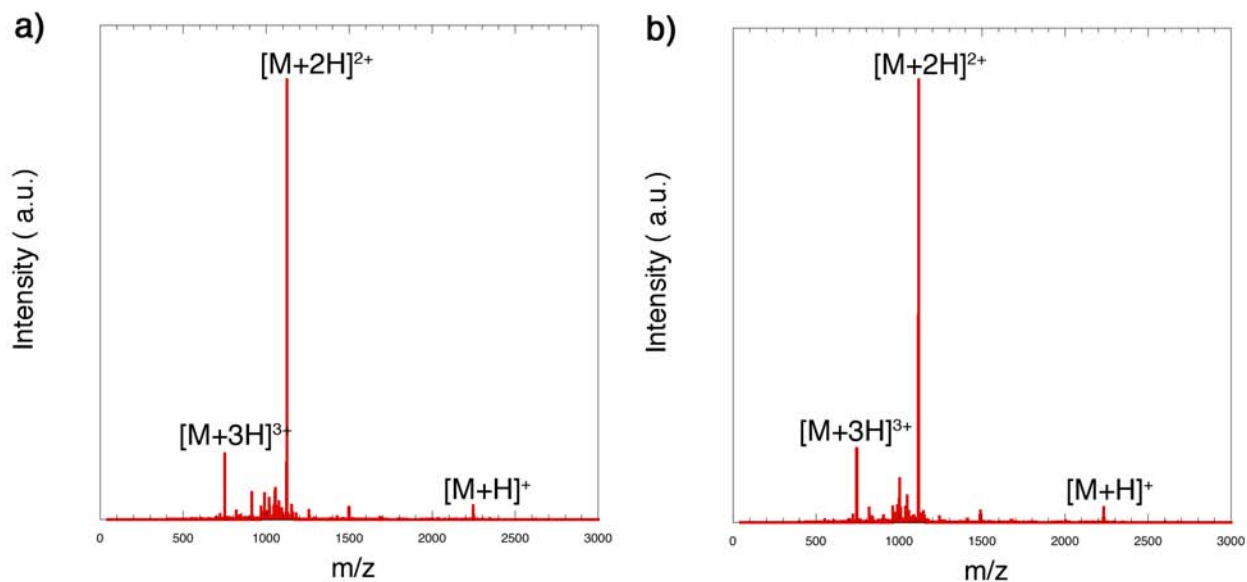
Figure S1. ESI-TOF mass spectrometry. Mass spectra of a) KGE peptide, $[M+2H]^{2+}$ expected = 1123.0 / observed = 1122.9 and b) KGD peptide, $[M+2H]^{2+}$ expected = 1116.0 / observed = 1115.6.
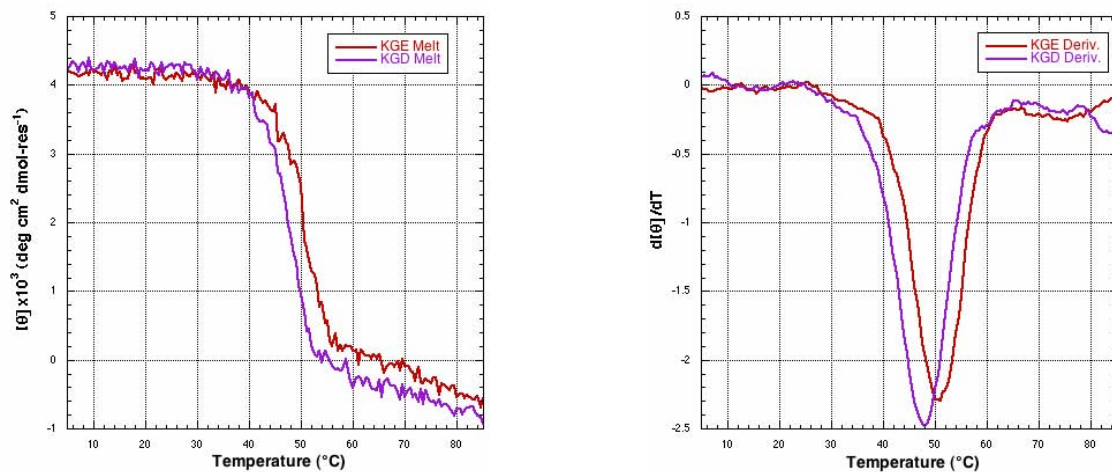
Figure S2. CD spectroscopy. CD melting curves and derivatives with respect to temperature for the a) **KGE** peptide and b) **KGD** peptide. Both measurement were carried out for 0.3 mM samples in 10 mM phosphate buffer at neutral pH and a scan rate of 10° C / hour.
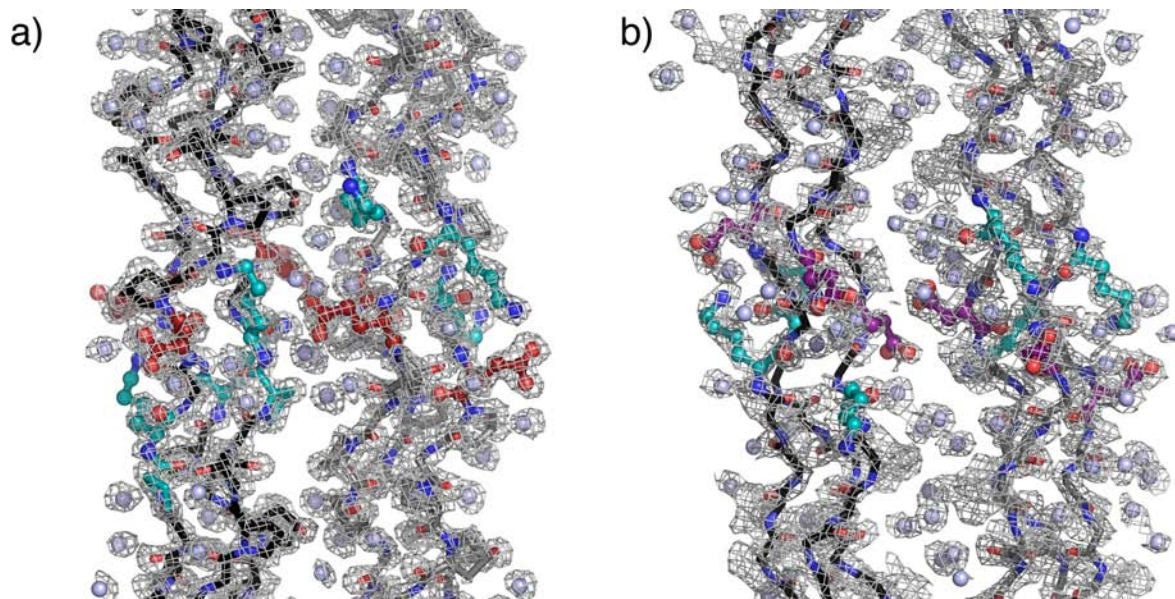
Figure S3. Atomic structure of **KGE** and **KGD**. a) Contents of the asymmetric unit of the **KGE** crystal. The 1.68 Å $2F_o$-F_c map contoured at 1.2σ is depicted as a wireframe surface. b) Contents of the asymmetric unit of the **KGD** crystal. The 2.00 Å $2F_o$-F_c map contoured at 1.2σ is depicted as a wireframe surface. The host regions shows the typical structure observed in triple helical peptides containing a high content of Pro-Hyp-Gly triplets, including the intra- and inter-chain hydration network involving Hyp residues(1) and the water mediated contacts involving the backbone amide of an residues in the Xxx position(2).
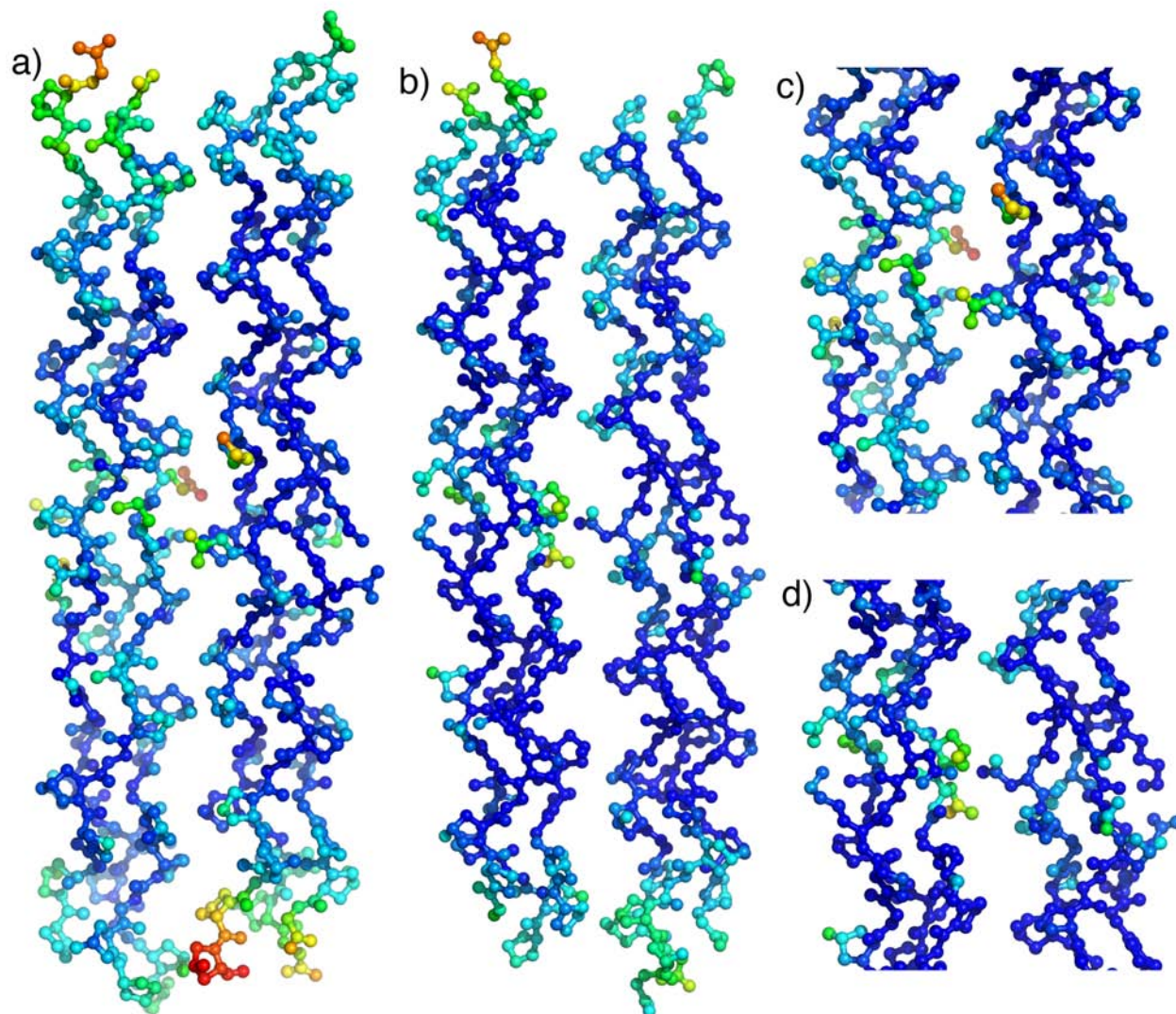
Figure S4. Overall structure of a) **KGE** and b) **KGD**. The guest regions of each triple helix are highlighted in panels c) and d) respectively. Atoms are colored by B-factors. Hotter colors signify higher B-factors. All of the side chain atoms of the charged residues in the guest region were included in the final model but some of them show a higher degree of flexibility, as evidenced by their high B-factors.
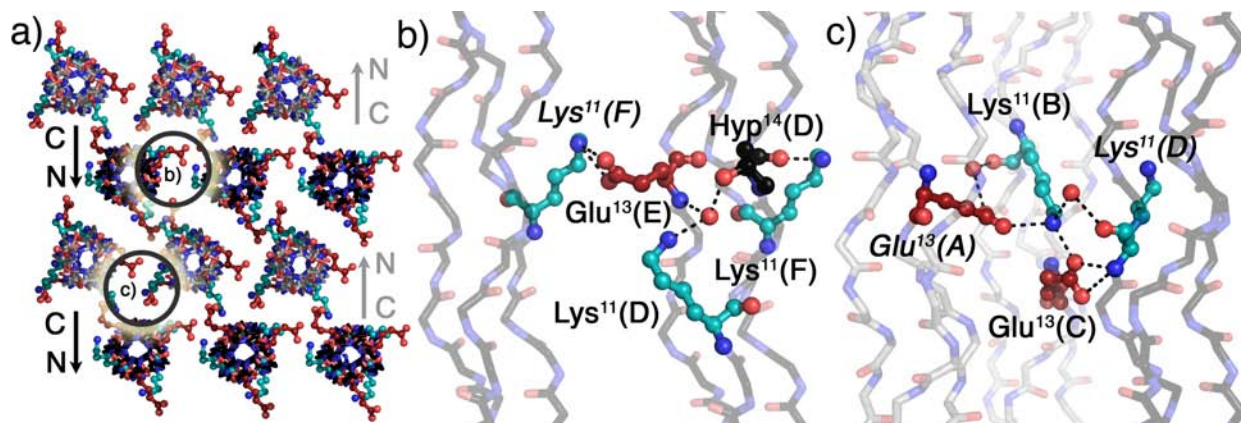
Figure S5. Crystal packing and Molecular interactions of **KGE**. a) Crystal packing of the **KGE** peptide highlighting the positions of the lysine(cyan) and glutamate (red) side-chains.). Side view of the areas highlighted by circles are depicted in the following panels. Triple helices oriented N- to C- terminus are shown in gray (A-leading chain, B-middle chain, C-lagging chain) and triple helices oriented C- to N- terminus in black (D-leading chain, E-middle chain, F-lagging chain). b), c) Inter- and intra-helical hydrogen bonding networks involving the charged side-chains at the interface of b) two parallel tripe helices and c) three anti-parallel triple helices. Amino acids are labeled using their three-letter code, sequence position and chain. Images generated using pymol.
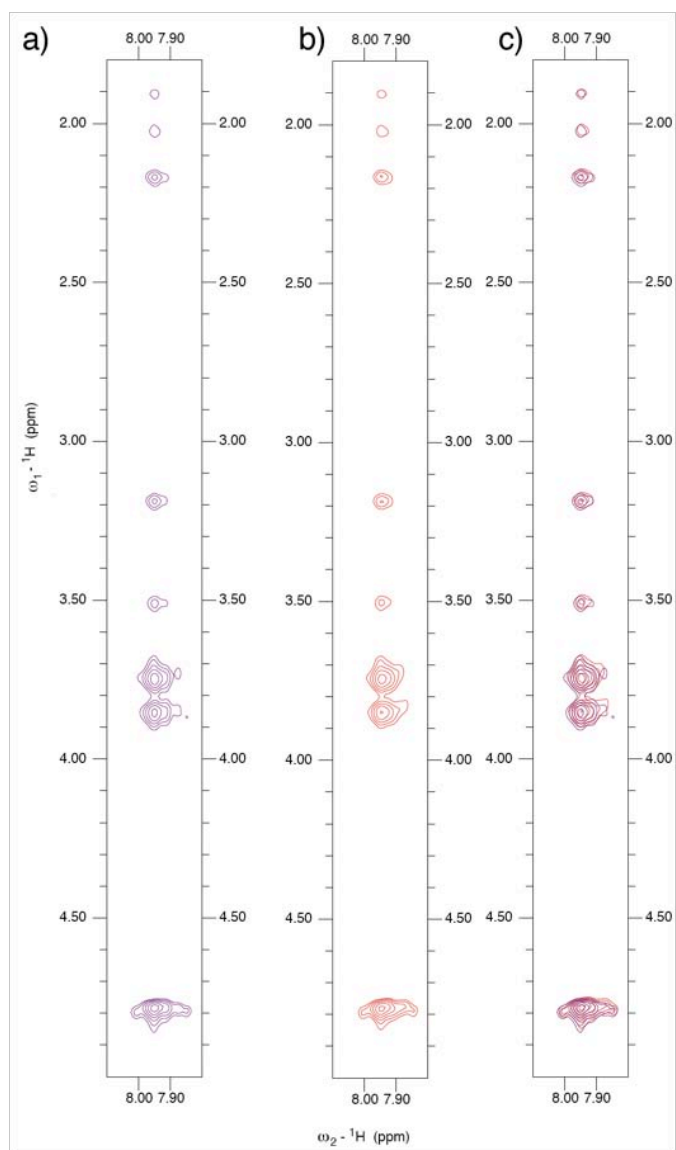
Figure S6. [1]H,[1]H-NOESY Spectra. Strip of the spectrum showing the chemical shift of glycine in the host region for a) **KGE** peptide, b) **KGD** peptide and c) overlay showing the similarity observed between the host regions of both peptides.

9
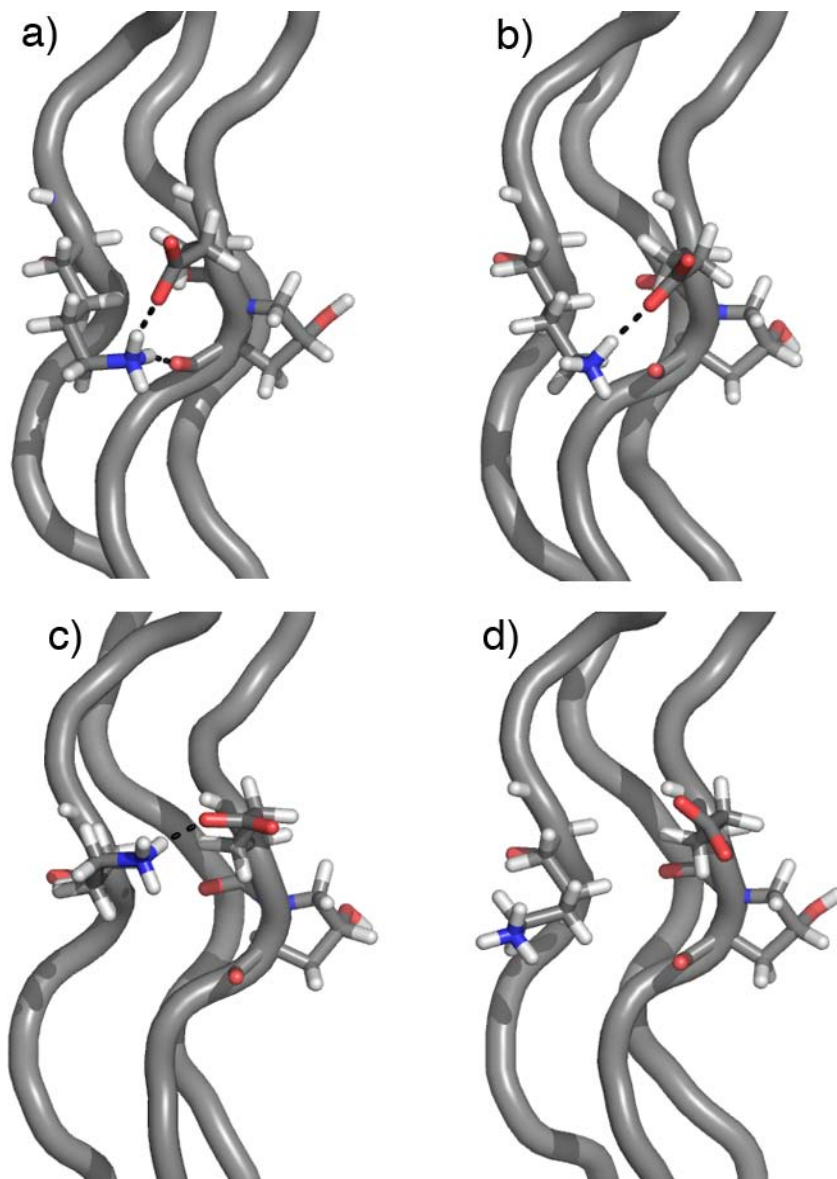
Figure S7. KGE Ensemble**.** Representative conformers highlighting the different possible interactions between the charged amino acids in the leading and lagging strands. a) Conformation participating in both the Lys[11](C)-Glu[13](A) salt bridge and Lys[11](C)-Hyp[14](A) polar contact (lowest energy conformer). b and c) Two alternative Lys[11](C)-Glu[13](A) salt bridge conformations. d) Conformer with no polar contacts involving the charged side chains.
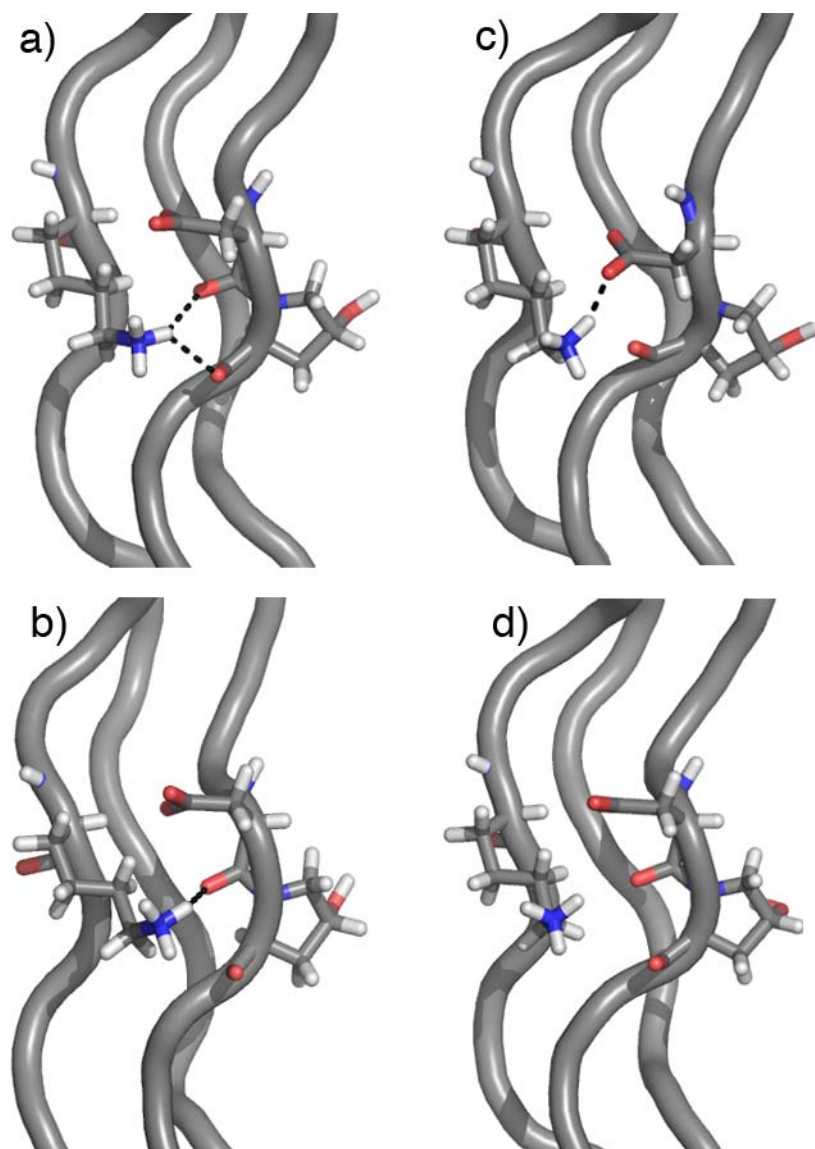
Figure S8. KGD Ensemble**.** Representative conformers highlighting the different possible interactions between the charged amino acids in the leading and lagging strands. a) Conformation participating in both the Lys[11](C)-Asp[13](A) and Lys[11](C)-Hyp[14](A) polar contacts (lowest energy conformer). b) Conformation showing exclusively the Lys[11](C)-Asp[13](A) polar contact. c) Lys[11](C)-Asp[13](A) salt bridge. d) Conformer with no polar contacts involving the charged side chains.

TABLE S1

Dihedrals calculated from the **KGE** crystal structure

	$\varphi(Xxx)$	$\psi Xxx)$	φ (Yyy)	ψ (Yyy)	φ (Gly)	ψ (Gly)
Host region[a]	-73.9 (3.3)	165.4 (5.4)	-58.7 (2.8)	150.0 (4.2)	-71.7 (3.5)	175.1 (4.2)
Guest region[b]	-70.8 (5.1)	157.4 (3.9)	-63.5 (4.6)	150.7 (4.3)	-71.4 (5.6)	171.6 (5.0)
$(POG)_{10}$[c]	-72.7 (3.5)	161.1 (5.1)	-58.4 (4.8)	154.9 (6.4)	-74.8 (5.6)	172.8 (3.0)
7/2 helix[d]	-77.9	166.1	-60.3	163.4	-75.7	176.3
10/3 helix[d]	-67.6	147.7	-69.0	155.4	-78.5	147.1

[a] Amino acids 4-9 and 16-21
[b] Amino acids 10-15
[c] Crystal structure at 1.9 Å resolution is from Nagarajan *et al.* (3)
[d] Models from Okuyama *et al.* (4)

TABLE S2
Constraints used for **KGE** NMR ensemble.

```
59    LYS   HG2   59    LYS   HA    2.20 3.20
37    GLU   HG2   37    GLU   HA    2.20 3.40
61    GLU   H     61    GLU   HB3   2.20 3.20
61    GLU   HG2   35    LYS   HE3   2.00 3.00
61    GLU   HG2   61    GLU   HA    2.20 3.20
11    LYS   HG2   11    LYS   HE3   2.30 3.50
37    GLU   H     37    GLU   HG2   2.30 3.50
37    GLU   HG2   11    LYS   HE2   2.00 3.00
13    GLU   H     13    GLU   HB2   1.90 2.90
37    GLU   HG2   37    GLU   HA    2.40 3.60
61    GLU   HB3   61    GLU   HA    1.90 2.90
35    LYS   HG2   35    LYS   HA    2.20 3.20
38    HYP   HD3   37    GLU   HA    1.80 2.60
13    GLU   H     13    GLU   HB3   2.20 3.20
37    GLU   HB2   37    GLU   HA    2.00 3.00
37    GLU   H     37    GLU   HB3   2.20 3.20
59    LYS   QD    59    LYS   QE    1.90 2.90
37    GLU   H     11    LYS   HE3   2.40 3.60
13    GLU   QG    13    GLU   HA    1.80 2.60
61    GLU   H     61    GLU   HG3   2.20 3.40
35    LYS   HG2   35    LYS   HE3   2.30 3.50
61    GLU   H     35    LYS   HE2   2.30 3.50
37    GLU   H     37    GLU   HB2   1.90 2.90
61    GLU   HB2   61    GLU   HA    1.80 2.80
11    LYS   H     11    LYS   HG2   2.30 3.50
13    GLU   HB2   13    GLU   HA    2.10 3.10
62    HYP   QD    61    GLU   HA    1.70 2.50
38    HYP   HD2   37    GLU   HA    1.80 2.60
37    GLU   HG2   11    LYS   HE2   1.80 2.80
37    GLU   H     37    GLU   HG2   2.20 3.20
37    GLU   HB3   37    GLU   HA    2.00 3.00
59    LYS   HG3   59    LYS   HA    2.00 3.00
35    LYS   H     35    LYS   HG2   2.30 3.50
61    GLU   H     61    GLU   HG2   2.10 3.10
12    GLY   H     11    LYS   HG3   2.10 3.10
13    GLU   H     13    GLU   QG    2.00 3.00
61    GLU   HG2   61    GLU   HA    2.30 3.50
61    GLU   H     35    LYS   HE3   2.20 3.40
14    HYP   HD3   13    GLU   HA    1.80 2.60
11    LYS   HG2   11    LYS   HA    2.20 3.20
37    GLU   H     11    LYS   HE2   2.40 3.60
13    GLU   HB3   13    GLU   HA    1.80 2.60
61    GLU   HG2   35    LYS   HE3   2.20 3.20
13    GLU   H     59    LYS   HA    2.20 3.20
36    GLY   H     35    LYS   HG2   2.20 3.40
12    GLY   H     11    LYS   HG2   2.20 3.40
36    GLY   H     35    LYS   HG3   2.10 3.10
59    LYS   HG2   59    LYS   QE    2.30 3.50
```

TABLE S3.
Constraints used for **KGD** NMR ensemble.

```
13    ASP   H       59    LYS   HA      2.20  3.20
12    GLY   H       12    GLY   HA2     1.90  2.90
11    LYS   HG3     11    LYS   HA      2.20  3.20
13    ASP   H       12    GLY   HA2     1.80  2.80
61    ASP   H       61    ASP   HB2     2.20  3.20
37    ASP   H       37    ASP   HB3     1.90  2.90
61    ASP   H       61    ASP   HA      2.20  3.40
60    GLY   H       59    LYS   HG3     2.30  3.50
61    ASP   H       35    LYS   QE      2.20  3.20
13    ASP   H       13    ASP   HB2     2.10  3.10
60    GLY   H       59    LYS   HG2     1.90  2.90
36    GLY   H       35    LYS   HA      1.70  2.50
13    ASP   H       12    GLY   HA3     1.90  2.90
13    ASP   H       13    ASP   HB3     1.80  2.80
37    ASP   H       37    ASP   HB2     2.20  3.20
35    LYS   HG3     35    LYS   HA      2.20  3.20
59    LYS   HG3     59    LYS   HA      2.20  3.40
61    ASP   H       60    GLY   HA3     2.00  3.00
36    GLY   H       35    LYS   HG2     2.00  3.00
12    GLY   H       11    LYS   HG3     2.20  3.20
61    ASP   H       60    GLY   HA2     1.90  2.90
12    GLY   H       11    LYS   HG2     2.00  3.00
36    GLY   H       35    LYS   HG3     2.20  3.20
60    GLY   H       59    LYS   HA      1.70  2.50
59    LYS   HG3     59    LYS   QE      2.30  3.50
37    ASP   H       37    ASP   HA      2.30  3.50
13    ASP   H       13    ASP   HA      2.20  3.40
35    LYS   HG3     35    LYS   QE      2.10  3.10
37    ASP   H       11    LYS   QE      2.20  3.20
11    LYS   HG3     11    LYS   QE      2.10  3.10
37    ASP   H       36    GLY   HA3     1.90  2.90
12    GLY   H       11    LYS   HA      1.70  2.50
61    ASP   H       61    ASP   HB3     1.90  2.90
37    ASP   H       36    GLY   HA2     1.90  2.90
```

Table S4.
Stereospecific assignments for the E37 β–protons using NOE cross peak intensities

	Gauche (+)	Trans	Gauche (-)	Observed
α – β2	~	+	-	-
α – β3	~	-	+	+
H – β2	-	~	+	+
H – β3	+	~	-	-

Table S5.
Stereospecific assignments for the E37 γ–protons using NOE cross peak intensities.

	Gauche (+)	Trans	Gauche (-)	Observed
β2 – γ2	-	+	~	~
β2 – γ3	+	-	~	~
H – γ2	~	+	-	-
H – γ3	~	-	+	+

Table S6.
NMR ensemble statistics

NMR constraints	KGE	KGD
Distance constraints		
Intra-residue	31	17
Sequential ($|i - j| = 1$)	10	15
Interchain	9	3
Structure statistics[a]		
Violations (mean±ds.d.)		
Distance constraints (Å)	0.005±d 0.001	0.005 ±d 0.001
Max. distance constraint violation (Å)	0.007	0.007
Average pairwise r.m.s. deviation[b]		
Backbone	0.81	0.93

[a] Calculated over all amino acids using utilities from the amber09 package
[b] Over 100 structures

References

1. Bella, J., B, B. and Berman, H. M. (1995) *Structure* **3**, 893-906
2. Kramer, R. Z., Bella, J., Mayville, P., Brodsky, B. and Berman, H. M. (1999) *Nat Struct Biol* **6**, 454-457
3. Nagarajan, V., Kamitori, S. and Okuyama, K. (1999) *J Biochem* **125**, 310-318
4. Okuyama, K., Xu, X. Z., Iguchi, M. and Noguchi, K. (2006) *Biopolymers* **84**, 181-191
5. Otwinowski, Z. and Minor, W. (1997) *Method Enzymol* **276**, 307-326
6. Kissinger, C. R., Gehlhaar, D. K. and Fogel, D. B. (1999) *Acta Crystallogr D* **55**, 484-491
7. Kramer, R. Z., Venugopal, M. G., Bella, J., Mayville, P., Brodsky, B. and Berman, H. M. (2000) *J. Mol. Biol.* **301**, 1191-1205
8. Brunger, A. T., Adams, P. D., Clore, G. M., DeLano, W. L., Gros, P., Grosse-Kunstleve, R. W., Jiang, J. S., Kuszewski, J., Nilges, M., Pannu, N. S., Read, R. J., Rice, L. M., Simonson, T. and Warren, G. L. (1998) *Acta Crystallogr D* **54**, 905-921
9. Emsley, P., Lohkamp, B., Scott, W. G. and Cowtan, K. (2010) *Acta Crystallogr D* **66**, 486-501
10. Kramer, R. Z., Bella, J., Brodsky, B. and Berman, H. M. (2001) *J. Mol. Biol.* **311**, 131-147
11. Murshudov, G. N., Vagin, A. A. and Dodson, E. J. (1997) *Acta Crystallogr D* **53**, 240-255
12. Delaglio, F., Grzesiek, S., Vuister, G. W., Zhu, G., Pfeifer, J. and Bax, A. (1995) *J. Biomol. NMR* **6**, 277-293
13. Vranken, W. F., Boucher, W., Stevens, T. J., Fogh, R. H., Pajon, A., Llinas, P., Ulrich, E. L., Markley, J. L., Ionides, J. and Laue, E. D. (2005) *Proteins* **59**, 687-696
14. Powers, R., Garrett, D. S., March, C. J., Frieden, E. A., Gronenborn, A. M. and Clore, G. M. (1993) *Biochemistry* **32**, 6744-6762
15. Delano, W. L. (2002) *The PyMOL Molecular Graphics System, Delano Scientific, San Carlos, CA, USA*
16. Case, D. A., Cheatham, T. E., Darden, T., Gohlke, H., Luo, R., Merz, K. M., Onufriev, A., Simmerling, C., Wang, B. and Woods, R. J. (2005) *J. Comput. Chem.* **26**, 1668-1688
17. Gurry, T., Nerenberg, P. S. and Stultz, C. M. (2010) *Biophys. J.* **98**, 2634-2643
18. Park, S., Radmer, R. J., Klein, T. E. and Pande, V. S. (2005) *J. Comput. Chem.* **26**, 1612-1616